Wind-proof and sand-fixing effects of *Artemisia ordosica* with different coverages in the Mu Us Sandy Land, northern China

PANG Yingjun[1,2,3,4*], WU Bo[1,2,3*], JIA Xiaohong[1,2,3], XIE Shengbo[5]

[1] Institute of Desertification Studies, Chinese Academy of Forestry, Beijing 100091, China;
[2] Institute of Ecological Conservation and Restoration, Chinese Academy of Forestry, Beijing 100091, China;
[3] Key Laboratory of Desert Ecosystem and Global Change, National Forestry and Grassland Administration, Beijing 100091, China;
[4] Kumtag Desert Ecosystem Research Station, National Forestry and Grassland Administration, Dunhuang 736200, China;
[5] Key Laboratory of Desert and Desertification, Northwest Institute of Eco-Environment and Resources, Chinese Academy of Sciences, Lanzhou 730000, China

Abstract: Wind erosion is a key global environmental problem and has many adverse effects. The Mu Us Sandy Land of northern China is characterized by an arid climate, where vegetation patches and bare sand patches are usually distributed mosaically, and aeolian activities occur frequently. Vegetation plays a significant role in controlling wind erosion. *Artemisia ordosica* is the most dominant native plant species in the Mu Us Sandy Land. It is urgent to study the wind-proof and sand-fixing effects of *Artemisia ordosica* in the Mu Us Sandy Land. This study analyzed the wind-proof and sand-fixing effects of *Artemisia ordosica* based on the field data of wind regimes, aeolian sediment transport, and surface change of *Artemisia ordosica* plots with four coverages (denoted as site A, site B, site C, and site D) in the Mu Us Sandy Land during the period from 1 June 2018 to 29 June 2019. The coverages of *Artemisia ordosica* at site A, site B, site C, and site D were 2%, 16%, 29%, and 69%, respectively. The annual average wind speeds at 2.0 m height above the ground for site A, site B, site C, and site D were 3.47, 2.77, 2.21, and 1.97 m/s, respectively. The annual drift potentials were 193.80, 69.72, 15.05, and 6.73 VU at site A, site B, site C, and site D, respectively. The total horizontal aeolian sediment fluxes during the period from 2–3 June 2018 to 6 June 2019 at site A, site B, site C, and site D were 4633.61, 896.80, 10.54, and 6.14 kg/m, respectively. Site A had the largest surface changes, and the surface changes at site B were significantly weaker than those at site A, whereas the surface changes at site C and site D were minimal. The results indicated that *Artemisia ordosica* significantly reduced the wind speed, drift potential, aeolian sediment transport, and surface changes. The higher the coverage of *Artemisia ordosica* is, the more obvious the effects of wind-proof and sand-fixing. Wind erosion would be effectively controlled in the Mu Us Sandy Land if the coverage of *Artemisia ordosica* is greater than 29%. These results provide a scientific basis for evaluating the ecosystem service function of *Artemisia ordosica* and the vegetation protection and construction projects in the Mu Us Sandy Land.

Keywords: *Artemisia ordosica*; wind-proof; sand-fixing; wind erosion; aeolian sediment flux; Mu Us Sandy Land

Citation: PANG Yingjun, WU Bo, JIA Xiaohong, XIE Shengbo. 2022. Wind-proof and sand-fixing effects of *Artemisia ordosica* with different coverages in the Mu Us Sandy Land, northern China. Journal of Arid Land, 14(8): 877–893. https://doi.org/10.1007/s40333-022-0070-4

*Corresponding authors: PANG Yingjun (E-mail: pangyingjun@caf.ac.cn); WU Bo (E-mail: wubo@caf.ac.cn)
Received 2022-02-14; revised 2022-06-06; accepted 2022-06-14

1 Introduction

Wind erosion is a global environmental problem that has many adverse effects, such as soil degradation, crop damage, and health problems (Leenders et al., 2011; Youssef et al., 2012; Asensio et al., 2016). Considering the adverse effects of wind erosion, there is a vital need to develop effective methods for its prevention. Mechanical methods such as straw checkerboards, nylon barriers, and chemical sand-fixing materials are commonly used to reduce the erosive forces of wind and minimize the sediment transport, however, ecological revegetation is still the most widely used approach. The effects of vegetation on aeolian sediment transport have long been recognized (Buckley, 1996). Vegetation plays a significant role in reducing wind erosion in arid and semi-arid environments (Burri et al., 2011). There is a degree of high confidence that a negative relationship exists between vegetation green-up and dust storm frequency (IPCC, 2019). Vegetation can reduce aeolian sediment transport by reducing the wind speed and soil erodibility and capturing the transported sediment particles (Leenders et al., 2011; Youssef et al., 2012; Leenders et al., 2016).

The flow regimes are determined by the element shape, width, height, spacing, and arrangement (Wolfe and Nickling, 1993). The wind speed on the leeward side of the vegetation element varied with its height, porosity, and downwind position. Leenders et al. (2011) indicated that the wind speed was recovered to the incoming flow speed downwind 7.5 times the height of shrubs. The results of field and wind tunnel studies implied that aeolian sediment flux decreases exponentially with the increase of vegetation coverage (Lancaster and Baas, 1998; Burri et al., 2011). Wind erosion reduction depends not only upon vegetation coverage but also on plant morphology and plant distribution relative to the wind direction (Dupont et al., 2014). Trees can reduce the wind speed more strongly than shrubs, but shrubs are more effective in trapping transported materials and protecting the surface under the canopy (Leenders et al., 2016). Furthermore, vegetation patterns influence the wind turbulence and play a significant role in aeolian sediment transport (Youssef et al., 2012). The vegetation type, density, and optimal arrangement demand further study to combat wind erosion effectively (Leenders et al., 2007). A minimal vegetation cover controlling wind erosion would reduce the revegetation cost and competition for limited water resources (Youssef et al., 2012). It is urgent to determine the proper density of sand-fixing plants that can not only prevent wind erosion but also save the input of labour and resources.

Shrubs are widely used in desertification control projects and play a very important role in controlling surface wind erosion. The commonly used sand-fixing shrubs in sandy areas of northern China include *Artemisia sphaerocephala*, *Artemisia halodendron*, *Alhagi sparsifolia*, *Hedysarum laeve*, *Salix gordejevii*, *Caragana intermedia*, *Caragana microphylla*, and *Sophora moorcroftiana* (Wang, 2003). The types of shrubs used in desertification control varied with climate and soil conditions (Ci and Yang, 2010). For example, the main shrubs used in the protective system of Shapotou section of the Baotou-Lanzhou Railway in Tengger Desert of northern China were *Artemisia ordosica*, *Hedysarum scoparium*, and *Caragana Korshinskii* (Li et al., 2004). For the Tarim Desert Highway shelterbelt located in an extremely arid area of northern China, the main planted shrubs were *Calligonum mongolicum*, *Tamarix chinensis*, and *Haloxylon ammodendron* (Lei et al., 2008).

The Mu Us Sandy Land is an important source of dust in northern China because of its fragile ecological environment, frequent human activities, and widespread desertified land (Sweeney et al., 2016; Feng et al., 2021). In recent decades, many ecological restoration projects have been implemented to prevent the expansion of desertification and improve the ecological environment in the Mu Us Sandy Land. Therefore, the normalized difference vegetation index (NDVI) increased significantly in this region (Sun et al., 2021). However, water resources in the Mu Us Sandy Land are in short supply and vegetation construction needs to consume many water resources, so determining how to balance the role of water resources and wind erosion prevention is very important. *Artemisia ordosica* is the most dominant native plant species in the Mu Us

Sandy Land, which covers approximately 31% of the total area and effectively stabilizes sand and provides favourable soil conditions for other perennials (Ohte et al., 2021). In addition, *Artemisia ordosica* can adapt to the arid sandy environment and is resistant to sand burial, wind erosion, and barrenness. It is also a commonly used artificial sand-fixing plant species. Therefore, it is very important to understand the wind-proof and sand-fixing effects of *Artemisia ordosica* with different coverages to determine the regions requiring revegetation and the proper density of revegetation. Direct experimental measurements in the field would be the simplest and most reliable approach (Buckley, 1987).

This study takes *Artemisia ordosica* as the research object by observing the wind speed and direction, aeolian sediment transport, and surface changes in the field plots with different *Artemisia ordosica* coverages and aims to (1) evaluate the wind-proof and sand-fixing effects of *Artemisia ordosica* in the Mu Us Sandy Land and (2) determine the suitable coverage of *Artemisia ordosica* for the purpose of preventing wind erosion and thus provide a scientific basis for the construction of regional ecological projects.

2 Study area and methods

2.1 Study area

The Mu Us Sandy Land, which is located in the transitional area between the southern part of the Ordos Plateau and the Loess Plateau of China, ranges from 37°27′ to 39°22′N and from 107°20′ to 111°30′E, with an elevation between 1200 and 1600 m and an area of approximately 4.0×10^4 km^2. The overview of the Mu Us Sandy Land is shown in Figure 1. The Mu Us Sandy Land is characterized by a temperate continental semi-arid climate (Zhang and Wu, 2020). The average annual precipitation is 250–440 mm, which is mainly concentrated between June and August and decreases from the southeast (SE) to the northwest (NW). The annual average temperature is 6.0°C–8.5°C. The vegetation patches and bare sand patches are usually distributed as mosaics. The Mu Us Sandy Land is characterized by sandstorm weather and the mean annual number of sandstorm days is 16 d. The sand-driving wind in the Mu Us Sandy Land is mainly oriented in the NW, north-northwest (NNW), and north (N) directions and mainly occurs from March to May. Cretaceous sandstones are widely distributed under the Ordos Plateau, and sand layers are contained in the surrounding loess. These sand materials are subjected to water and wind erosion and can provide a rich sand source material basis for the formation of the Mu Us Sandy Land. *Artemisia ordosica* is the most widely distributed plant species in the Mu Us Sandy Land.

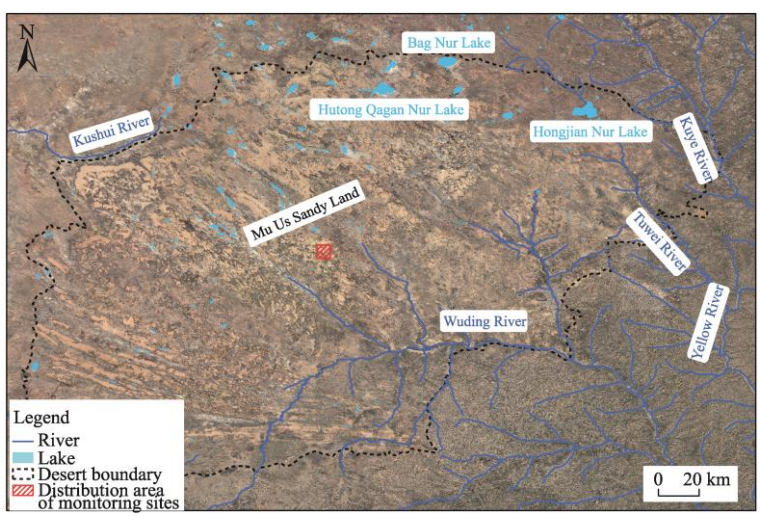

Fig. 1 Overview of the study area and distribution area of monitoring sites. Note that this map is based on the Google Earth images.

2.2 Methods

2.2.1 Vegetation and soil surveys

Four monitoring sites (A, B, C, and D) with different *Artemisia ordosica* coverages were chosen for this study. Based on the images at the four monitoring sites collected by the unmanned aerial vehicle (PHANTOM 4 RTK; SZ DJI Technology Co. Ltd., Shenzhen, China), the coverage of *Artemisia ordosica* at each monitoring site was calculated using the unsupervised classification method by the ENVI (Environment for Visualizing Images) software. The flight altitude of the unmanned aerial vehicle was approximately 100.0 m above the ground surface, and the spatial resolution of the images was approximately 3 cm. The quadrat areas for calculating the *Artemisia ordosica* coverages were 30 m×30 m. The coverage of *Artemisia ordosica* was approximately 2% at site A, 16% at site B, 29% at site C, and 69% at site D (Fig. 2; Table 1).

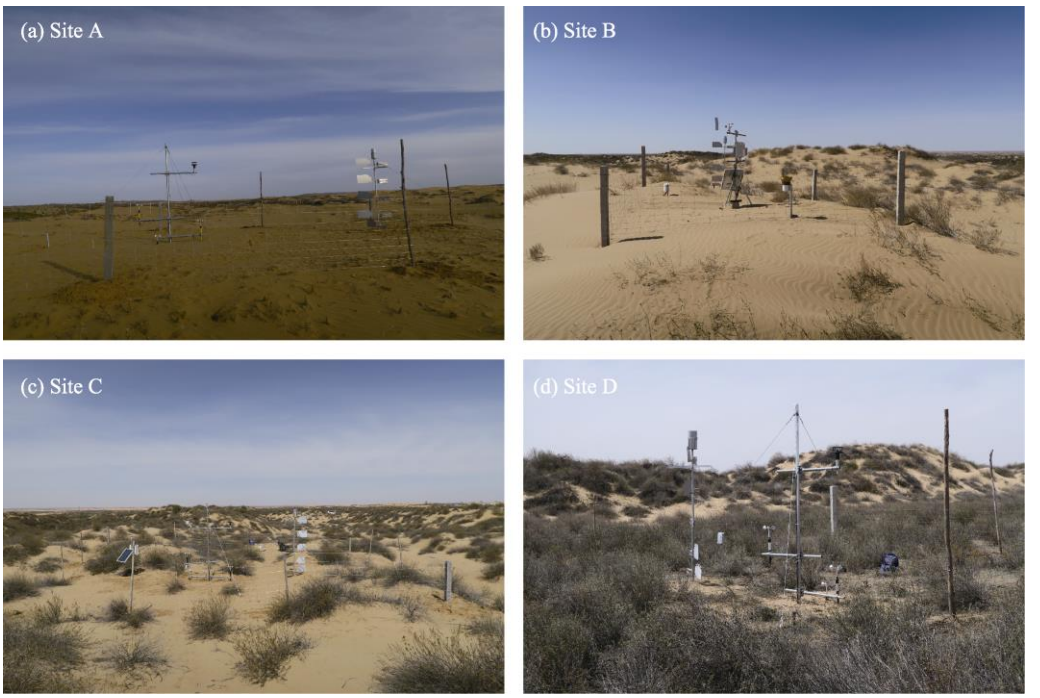

Fig. 2 Photographs of the monitoring sites with different coverages of *Artemisia ordosica*. (a), site A; (b), site B; (c), site C; (d), site D.

Table 1 Description of the monitoring sites selected in this study

Location	*Artemisia ordosica* coverage (%)	Observation height of wind (m)	Observation height of sediment collection (m)
Site A	2	0.2, 0.5, 1.0, and 2.0	0.2, 0.5, 1.0, 1.5, and 2.0
Site B	16	2.0	0.2, 0.5, 1.0, and 2.0
Site C	29	0.2, 0.5, 1.0, and 2.0	0.2, 0.5, 1.0, 1.5, and 2.0
Site D	69	0.2, 0.5, 1.0, and 2.0	0.2, 0.5, 1.0, 1.5, and 2.0

To understand the *Artemisia ordosica* community, we set up one 20 m×20 m, 12 m×14 m, and 12 m×10 m shrub quadrats at site B, site C, and site D in June 2018, respectively. The density of *Artemisia ordosica* at site A was too low, so *Artemisia ordosica* was not investigated at this site. The length, width of the crown, and height of each *Artemisia ordosica* in the quadrat were observed and recorded. The crown areas of *Artemisia ordosica* were calculated by the ellipse area formula. One 1 m×1 m herbaceous quadrat was set up at each site. The densities of *Artemisia ordosica* at site B, site C, and site D were 0.40, 0.46, and 1.34 plants/m^2, respectively. The crown

areas of *Artemisia ordosica* at site B, site C, and site D were 0.65, 0.68, and 0.43 m^2, respectively. The *Artemisia ordosica* heights at site B, site C, and site D were 0.37, 0.57, and 0.51 m, respectively. The amounts of herbaceous plants at site A, site B, and site C were all small, whereas there were a few herbaceous plants at site D. It should be also noted that biological crusts only existed at site D.

A sample line was set up at each site for collecting soil samples, and a surface sediment sample (0–5 cm) was collected every 5 m along the sample line in June 2018. Fourteen surface sediment samples were collected from site A, and eight surface sediment samples were respectively collected from site B, site C, and site D.

2.2.2 Observations of wind regime, aeolian sediment transport, and surface changes

Site A, site C, and site D were each equipped with a wind monitoring tower. The wind speeds at heights of 0.2, 0.5, and 1.0 m above the ground were measured by wind sensors (010C; Met One Instruments, Inc., Washington, USA), and the wind speeds and directions at a height of 2.0 m were measured by ultrasonic anemometers (WindSonic, Gill Instruments Limited, Hampshire, UK). Only the wind speeds and directions at a height of 2.0 m at site B were observed by wind sensor (034B; Met One Instruments, Inc., Washington, USA). The wind data were collected at 10-min intervals during the observation period from 1 June 2018 to 6 June 2019.

Horizontal aeolian sediment samples were collected by the Big Spring Number Eight (BSNE) samplers at heights of 0.2, 0.5, 1.0, 1.5, and 2.0 m at all monitoring sites, except for site B (Table 1). There were no BSNE samplers at 1.5 m height for site B, but the BSNE samplers at other heights were available. The entrance size of the BSNE sampler was 2 cm×5 cm. The BSNE samplers have been monitored since 2–3 June 2018, and the samples were collected on 20–21 July 2018, 5 September 2018, 1 December 2018, 5 January 2019, 1 March 2019, 6 April 2019, 8 May 2019, and 6 June 2019. The horizontal aeolian sediment samples collected on 6 April 2019, 8 May 2019, and 6 June 2019 were mixed. The grain size distributions for the surface sediment and the mixed aeolian sediment samples were measured by a Mastersizer 3000 laser diffraction grain size analyser (Malvern Panalytical Ltd., Malvern, Worcestershire, UK).

To determine the underlying surface changes, we set a surface erosion observation line at each site and inserted a straight iron pin into the ground every 5 m. Site A was equipped with 15 iron pins numbered A1, A2, A3, A4, A5, A6, A7, A8, A9, A10, A11, A12, A13, A14, and A15, and site B was equipped with 13 iron pins numbered B1, B2, B3, B4, B5, B6, B7, B8, B9, B10, B11, B12, and B13. The 13 iron pins numbered C1, C2, C3, C4, C5, C6, C7, C8, C9, C10, C11, C12, and C13, were set at site C, and the nine iron pins numbered D1, D2, D3, D4, D5, D6, D7, D8, and D9 were set at site D. The heights of the iron pins above the ground were measured with a tape measure on 2 June 2018, 20 July 2018, 5 September 2018, 1 December 2018, 1 March 2019, 6 April 2019, 8 May 2019, and 29 June 2019.

2.2.3 Calculations and statistics of grain size, wind data, drift potential (DP), and aeolian sediment flux

The grain size classification of the surface sediment and horizontal aeolian sediment samples was mainly followed the Udden-Wentworth classification standards (Udden, 1914; Wentworth, 1922). We then calculated the grain size parameters according to the method of Folk and Ward (1957).

The statistics of wind data were performed in 16 directions (N, north-northeast (NNE), northeast (NE), east-northeast (ENE), east (E), east-southeast (ESE), SE, south-southeast (SSE), south (S), south-southwest (SSW), southwest (SW), west-southwest (WSW), west (W), west-northwest (WNW), NW, and NNW). The abbreviation and the corresponding azimuth degree are shown in Table 2.

The DP is an important index to measure the regional aeolian activity intensity (Pang et al., 2020). The DPs were calculated using the wind data at the four monitoring sites by the following equation (Fryberger and Dean, 1979):

$$\mathrm{DP} = V^2 \times (V - V_t) \times t\,, \tag{1}$$

Table 2 Description of the direction and azimuth degree

Direction	Abbreviation	Azimuth degree (°)	Direction	Abbreviation	Azimuth degree (°)
North	N	348.75–11.25	South	S	168.75–191.25
North-northeast	NNE	11.25–33.75	South-southwest	SSW	191.25–213.75
Northeast	NE	33.75–56.25	Southwest	SW	213.75–236.25
East-northeast	ENE	56.25–78.75	West-southwest	WSW	236.25–258.75
East	E	78.75–101.25	West	W	258.75–281.25
East-southeast	ESE	101.25–123.75	West-northwest	WNW	281.25–303.75
Southeast	SE	123.75–146.25	Northwest	NW	303.75–326.25
South-southeast	SSE	146.25–168.75	North-northwest	NNW	326.25–348.75

where V is the wind speed (in knot; 1 knot≈0.51 m/s) above V_t (V_t is the threshold wind speed to move sand at 2.0 m height above the ground (9.72 knots)); and t is the frequency of sand-driving wind (%), which is expressed as a percentage of one year time. The resultant drift potential (RDP) and the resultant drift direction (RDD) were also calculated. The DP and RDP are both in vector units (VU).

In the present experiments, the exponential law expression was used to describe the vertical distribution of the horizontal aeolian sediment flux by the BSNE samplers:

$$q(z) = a \times e^{b \times z}, \tag{2}$$

where $q(z)$ is the aeolian sediment flux (kg/m^2); a and b are the fitted parameters; e is the natural constant; and z is the height of the opening of the BSNE sampler above the ground surface (m).

The total horizontal aeolian sediment flux (kg/m) for the sampling period can be calculated as follows:

$$G = \int_0^z q(z)\mathrm{d}z, \tag{3}$$

where G is the horizontal aeolian sediment flux per unit width (kg/m).

2.3 Statistical analysis

The data fitting and integration were performed by MATLAB R2018a, and data visualizations were done by OriginPro 9.1.

3 Results

3.1 Wind regime

The wind rose diagrams of the four monitoring sites at 2.0 m height above the ground in the Mu Us Sandy Land during the period from 1 June 2018 to 31 May 2019 (Fig. 3) showed that the wind direction distributions were similar, but the wind speeds varied greatly. The wind frequencies in the SE, NNW, and ESE directions were dominant for site A, accounting for 15.27%, 11.50%, and 11.14%, respectively. The wind frequencies in the SE, NW, and ESE directions were dominant for site B, accounting for 11.69%, 11.54%, and 10.38%, respectively. The wind frequencies in the SE, SSE, and N directions were dominant for site C, accounting for 15.02%, 12.28%, and 9.13%, respectively. The wind frequencies in the SE, NNW, and ESE directions were dominant for site D, accounting for 15.55%, 11.05%, and 10.66%, respectively. The frequency of the wind speeds greater than 5.00 m/s was the largest at site A, with the value of 21.33%, while it was the lowest at site D, with the value of 2.29%. The frequencies of the wind speeds greater than 5.00 m/s for site B and site C were between site A and site D, at 11.63% and 3.67%, respectively. The wind with speeds greater than 5.00 m/s was mainly concentrated in the NW, NNW, N, ESE, SE, and SSE directions at site A, WNW, NW, NNW, ESE, SE, and SSE directions at site B, NW, NNW, and N directions at site C, and NW and NNW directions at site D.

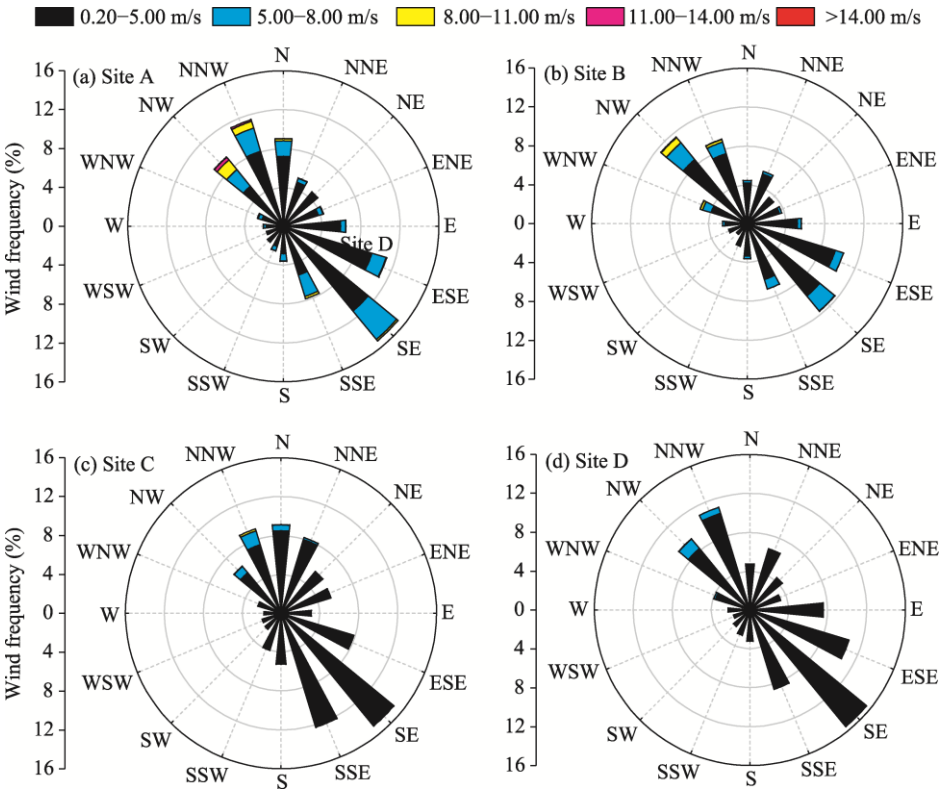

Fig. 3 Wind roses of the four monitoring sites at 2.0 m height above the ground during the period from 1 June 2018 to 31 May 2019. (a), site A; (b), site B; (c), site C; (d), site D. N, north; NNE, north-northeast; NE, northeast; ENE, east-northeast; E, east; ESE, east-southeast; SE, southeast; SSE, south-southeast; S, south; SSW, south-southwest; SW, southwest; WSW, west-southwest; W, west; WNW, west-northwest; NW, northwest; NNW, north-northwest.

Figure 4 shows the monthly average wind speeds at a height of 2.0 m above the ground for the four monitoring sites during the period from 1 June 2018 to 31 May 2019. The variation trends of the monthly average wind speeds at the four monitoring sites were similar. The average wind speeds in April, May, and July were greater for the four monitoring sites. The annual average wind speeds at the four monitoring sites (A, B, C, and D) were 3.47, 2.77, 2.21, and 1.97 m/s, respectively. In general, the wind speeds at the four monitoring sites showed the following descending order: site A>site B>site C>site D.

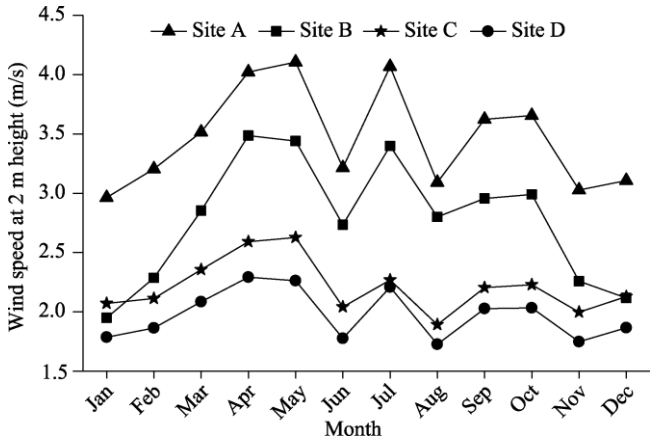

Fig. 4 Monthly average wind speeds at a height of 2.0 m above the ground at the four monitoring sites during the period from 1 June 2018 to 31 May 2019

3.2 DP

The distributions of the DPs at the four monitoring sites during the period from 1 June 2018 to 31 May 2019 calculated by Equation 1 are shown in Figure 5. The annual DPs at the four monitoring sites varied greatly. The annual DPs and RDPs both decreased with increasing *Artemisia ordosica* coverage. The annual DPs at site A, site B, site C, and site D were 193.80, 69.72, 15.05, and 6.73 VU, respectively. The annual RDPs at site A, site B, site C, and site D were 95.57, 43.67, 14.03, and 6.38 VU, respectively. The annual RDDs at the four monitoring sites were similar and ranged from 138.77° to 158.95°. The DPs at site A, site B, and site D were dominant in the NW direction, accounting for 40.44%, 44.54%, and 59.68% of the total annual DPs, respectively. The DP at site C was dominant in the NNW direction, occupying 65.06% of the total annual DP. The DP at site A was secondary high in the NNW direction, accounting for 23.65% of the total. The DP at site B was secondary high in the NNW and WNW directions, accounting for 18.27% and 14.99% of the total, respectively. The DP at site C was secondary high in the N and NW directions, accounting for 15.77% and 14.14% of the total, respectively. Further, the DP at site D was secondary high in the NNW direction, accounting for 31.86% of the total.

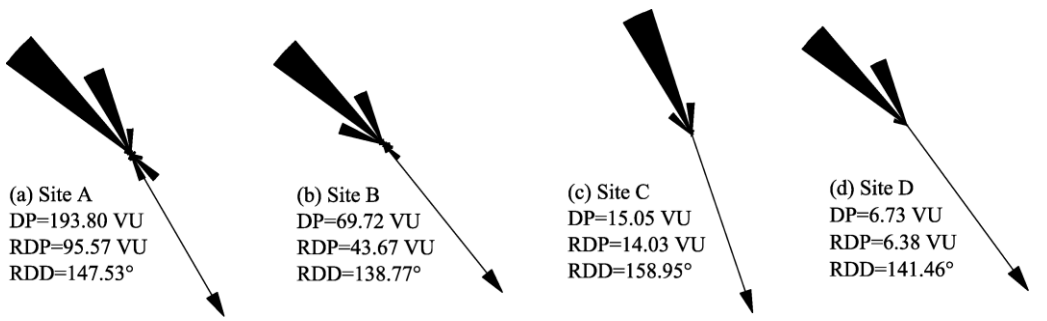

Fig. 5 Drift potential (DP) roses at the four monitoring sites during the period from 1 June 2018 to 31 May 2019. (a), site A; (b), site B; (c), site C; (d), site D. The arrow line segment represents the resultant drift potential (RDP), and the direction of the arrow represents the resultant drift direction (RDD). VU, vector units.

3.3 Horizontal aeolian sediment flux

The horizontal aeolian sediment flux at each height can be fitted by Equation 2, and the total horizontal aeolian sediment flux during the observation period was determined by Equation 3. Generally speaking, the horizontal aeolian sediment fluxes varied greatly for the four monitoring sites in the Mu Us Sandy Land (Fig. 6). During the period from 2–3 June 2018 to 6 June 2019, the total horizontal aeolian sediment fluxes at site A, site B, site C, and site D were 4633.61, 896.80, 10.54, and 6.14 kg/m, respectively. At site A and site B, the total horizontal aeolian sediment flux and daily horizontal aeolian sediment flux in spring (from March to May) were significantly greater than those in other seasons.

3.4 Grain size

The grain size data of the surface sediment samples for the same site were averaged. The surface sediment samples at the four monitoring sites were mainly composed of medium and fine sand (Table 2). The contents of very fine sand, silt, and clay in the surface sediment samples increased with increasing *Artemisia ordosica* coverage. Therefore, the contents of very fine sand, silt, and clay of the surface sediment samples at site D were higher than those at the other three monitoring sites. The mean grain size of the surface sediment samples at site B was highest, with the value of 293.79 μm, whereas it was lowest at site D, with the value of 150.81 μm. The mean grain sizes of the surface sediment samples at site A and site C were 272.94 and 267.66 μm, respectively.

The clay, coarse sand, very coarse sand, and gravel contents of the horizontal aeolian sediment samples at the four monitoring sites were very low (Table 2). The main component was fine sand for the horizontal aeolian sediment samples collected at different heights above the ground at site

A. For site B, the main component was medium sand for the horizontal aeolian sediment samples collected at 0.2 m height, fine sand for the samples collected at 0.5 and 1.0 m heights, and silt for the samples collected at 2.0 m height. For site C, the main component was medium sand for the horizontal aeolian sediment samples collected at 0.2 and 1.5 m heights, fine sand for the samples

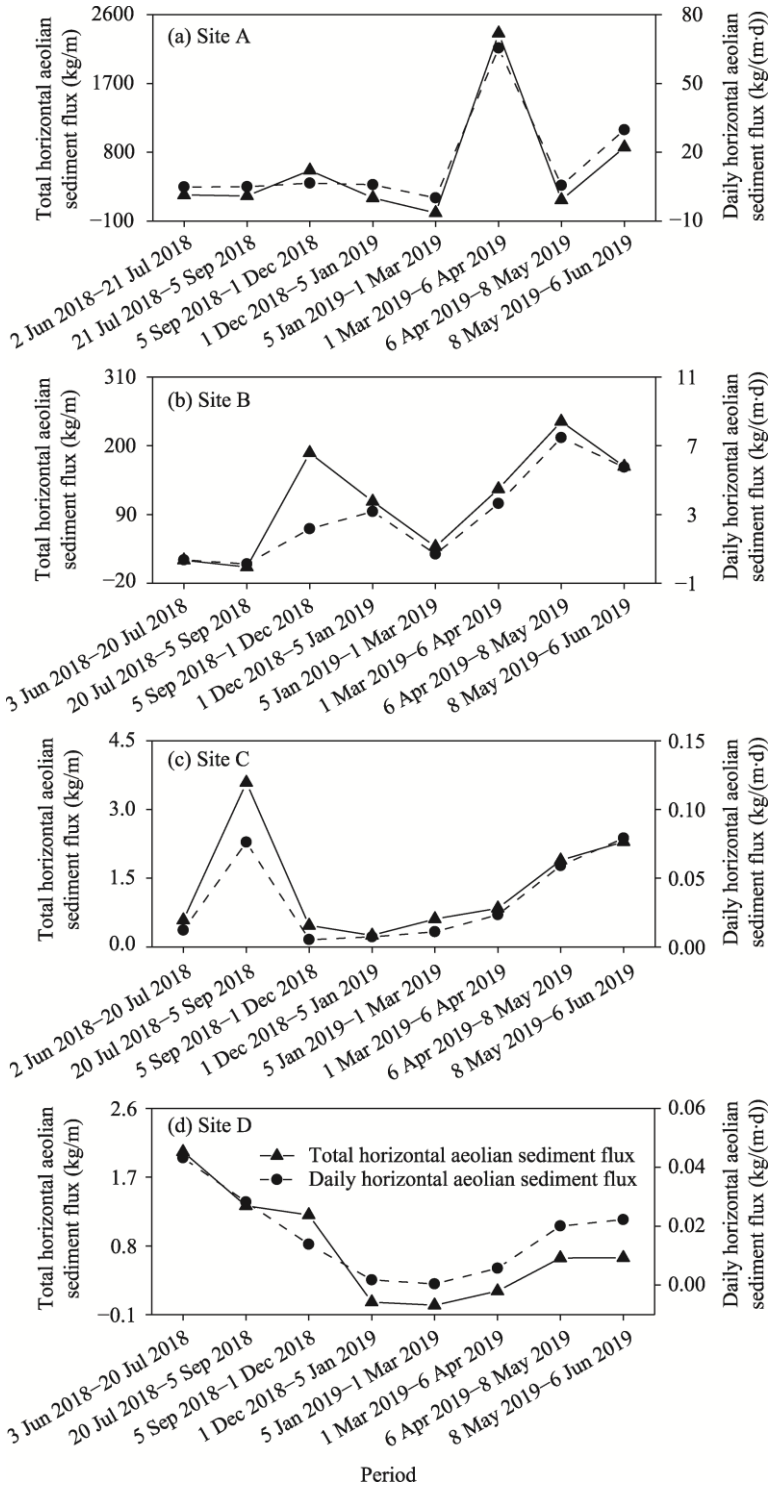

Fig. 6 Horizontal aeolian sediment fluxes at the four monitoring sites during the period from 2–3 June 2018 to 6 June 2019. (a), site A; (b), site B; (c), site C; (d), site D.

Table 2 Grain size distributions of the surface sediment samples and horizontal aeolian sediment samples at different heights above the ground

Location	Sample	Height above the ground (m)	Percentage of grain size (%)								Mean grain size (μm)
			Clay (0–2 μm)	Silt (2–63 μm)	Very fine sand (63–125 μm)	Fine sand (125–250 μm)	Medium sand (250–500 μm)	Coarse sand (500–1000 μm)	Very coarse sand (1000–2000 μm)	Gravel (>2000 μm)	
Site A	SSS	0.0	0.00	0.81	2.00	44.24	50.88	2.06	0.01	0.00	272.94
	HASS	0.2	0.00	0.00	3.24	54.03	41.45	1.28	0.00	0.00	234.24
	HASS	0.5	0.00	4.53	14.04	50.71	30.44	0.28	0.00	0.00	192.67
	HASS	1.0	0.00	3.83	21.68	55.09	19.40	0.00	0.00	0.00	168.06
	HASS	1.5	0.00	11.90	24.51	47.78	15.80	0.01	0.00	0.00	143.11
	HASS	2.0	0.00	11.27	23.57	49.77	15.38	0.00	0.00	0.00	145.43
Site B	SSS	0.0	0.05	2.38	1.82	36.27	52.71	6.77	0.00	0.00	293.79
	HASS	0.2	0.00	0.00	2.39	43.25	49.29	5.06	0.00	0.00	261.83
	HASS	0.5	0.00	1.23	6.24	52.53	38.58	1.43	0.00	0.00	224.38
	HASS	1.0	0.00	6.20	9.89	50.24	33.11	0.57	0.00	0.00	201.48
	HASS	2.0	0.01	45.99	25.45	20.82	7.59	0.15	0.00	0.00	73.06
Site C	SSS	0.0	0.00	2.28	3.80	42.98	46.98	3.96	0.00	0.00	267.66
	HASS	0.2	0.00	2.21	1.51	36.01	54.70	5.56	0.00	0.00	275.73
	HASS	0.5	0.00	16.46	19.87	39.33	23.79	0.54	0.00	0.00	143.39
	HASS	1.0	0.00	22.94	26.33	33.51	16.77	0.45	0.00	0.00	118.50
	HASS	1.5	0.00	22.64	19.43	22.25	25.71	9.89	0.09	0.00	151.78
	HASS	2.0	0.00	43.24	30.97	17.73	7.72	0.34	0.00	0.00	77.72
Site D	SSS	0.0	0.15	21.07	10.68	34.85	31.25	2.00	0.00	0.00	150.81
	HASS	0.2	0.00	19.63	19.97	34.27	23.46	2.66	0.02	0.00	138.16
	HASS	0.5	0.00	47.30	25.65	17.51	8.55	0.99	0.00	0.00	71.02
	HASS	1.0	0.01	64.01	23.85	9.32	2.80	0.01	0.00	0.00	45.94
	HASS	1.5	0.01	62.36	24.36	9.36	3.45	0.46	0.00	0.00	49.00
	HASS	2.0	0.00	50.74	28.81	12.90	6.05	1.49	0.00	0.00	66.47

Note: SSS, surface sediment sample; HASS, horizontal aeolian sediment sample.

collected at 0.5 and 1.0 m heights, and silt for the samples collected at 2.0 m height. For site D, the main component was fine sand for the horizontal aeolian sediment samples collected at 0.2 m height, and silt for the samples collected between 0.5 and 2.0 m heights. Except for the samples collected at 1.5 m height at site C, the medium sand contents of the horizontal aeolian sediment samples at site A, site B, and site C decreased with increasing height, but the silt and very fine sand contents increased with increasing height. Below 1.0 m height, the medium and fine sand contents of the horizontal aeolian sediment samples at site D decreased with increasing height, while the silt content increased with increasing height. For the same site, the mean grain sizes of the horizontal aeolian sediment samples tended to become finer with increasing height, and this trend was especially obvious at site A and site B. For the same sample collection height, the mean grain sizes of the horizontal aeolian sediment samples collected below 1.0 m height at site B were coarser than those at site A, whereas the mean grain sizes of the horizontal aeolian sediment samples collected above 1.0 m height at site B were finer than those at site A. For the same sample collection height, the mean grain sizes of the horizontal aeolian sediment samples

collected at 0.5 and 1.0 m heights at site C were finer than those at site A and site B. Compared with site A, site B, and site C, the mean grain sizes of the horizontal aeolian sediment samples at site D were finest at the same height. There was a finer trend in the horizontal aeolian sediment samples with the increase in *Artemisia ordosica* coverage, especially for the samples collected above 0.5 m height.

The grain size distributions of the surface sediment samples at site A, site B, and site C showed unimodal distribution curves, whereas the distribution showed a bimodal curve at site D (Fig. 7). The grain size distribution of the surface sediment samples was mainly concentrated in the ranges of 81.20–711.00 μm at site A, 81.20–807.50 μm at site B, 71.45–807.50 μm at site C, and 13.60–81.20 and 81.20–711.00 μm at site D. The peak grain sizes of the surface sediment samples at site A, site B, and site C were all approximately 291.00 μm. The two peak grain sizes were 42.85 and 225.50 μm at site D, respectively.

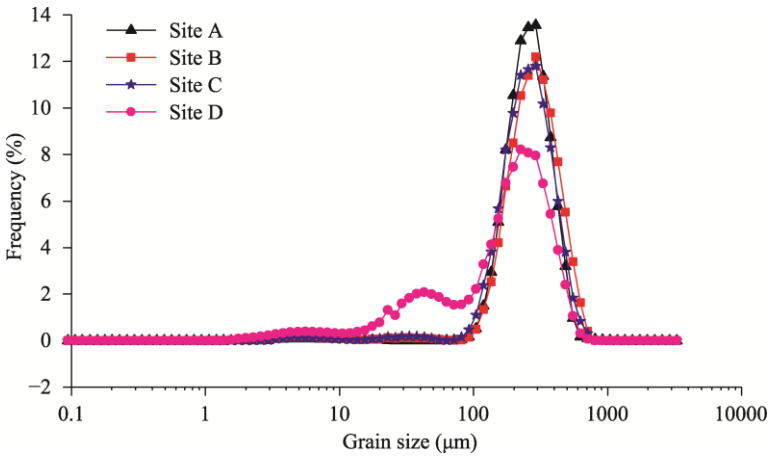

Fig. 7 Grain size distributions of the surface sediment samples at the four monitoring sites

In general, the grain size distributions of the horizontal aeolian sediment samples collected at different heights at the four monitoring sites in the Mu Us Sandy Land all showed unimodal distribution curves, except for the samples at 1.5 m height above the ground at site C (Fig. 8). However, the concentration distribution range and peak size of the aeolian sediment samples varied greatly. For the same site, the fine-grained material composition increased with increasing height, especially at site A, site B, and site C. The grain sizes of the horizontal aeolian sediment samples at site C and site D were significantly finer than those at site A and site B at the same height. The fine-grained material compositions ranged from 10 to 100 μm at site C and site D and were obviously higher than those at site A and site B at the same height.

3.5 Surface changes

The surface changes varied greatly for the four monitoring sites with different *Artemisia ordosica* coverages in the Mu Us Sandy Land during the period from 2 June 2018 to 29 June 2019 (Fig. 9). Site A had the largest change in the surface, with the maximum wind erosion depth of 35.4 cm and the maximum sand burial thickness of 64.1 cm. The surface changes at site B were significantly weaker, with the maximum wind erosion depth of 15.1 cm and the maximum sand burial thickness of 19.8 cm. For site C and site D, the surface changes were minimal.

4 Discussion

4.1 Relationship between the DP and horizontal aeolian sediment flux

The DPs for all observed sampling periods were calculated using Equation 1 to investigate the relationship between the DP and horizontal aeolian sediment flux. The DPs and horizontal aeolian

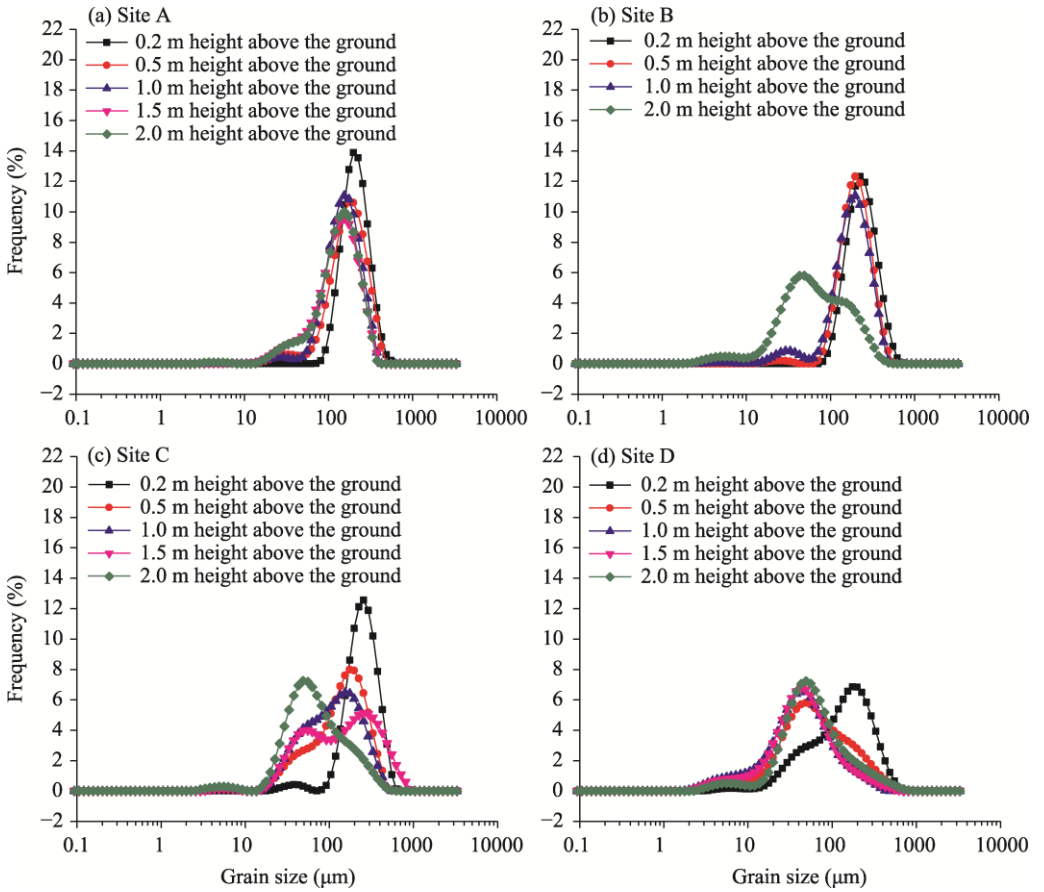

Fig. 8 Grain size distributions of the horizontal aeolian sediment samples at different heights at the four monitoring sites. (a), site A; (b), site B; (c), site C; (d), site D.

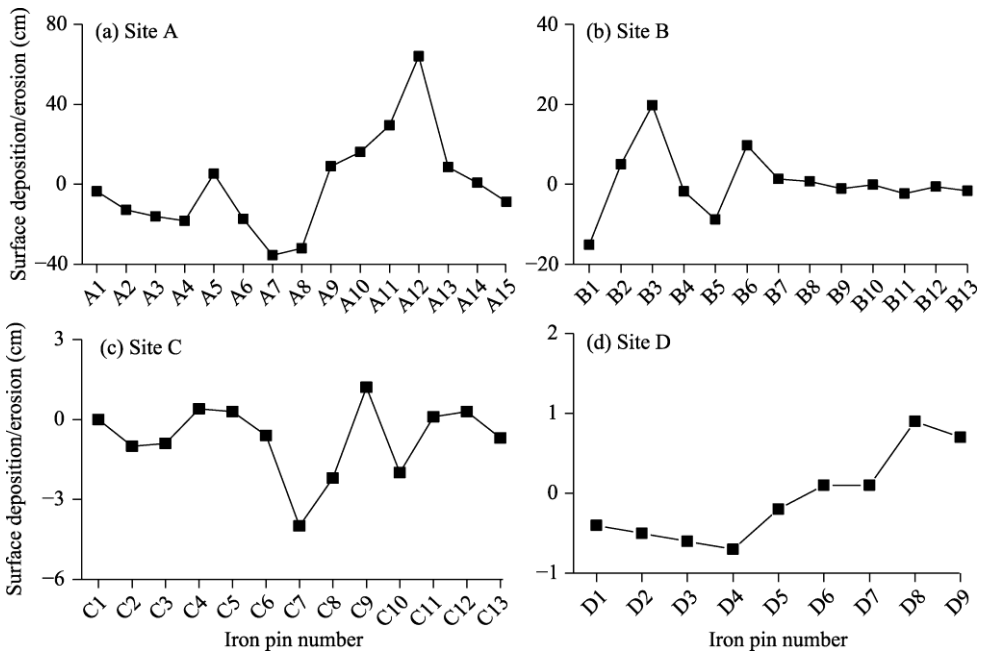

Fig. 9 Surface changes at the four monitoring sites during the period from 2 June 2018 to 29 June 2019. (a), site A; (b), site B; (c), site C; (d), site D. Positive values on *y*-axis represent surface deposition, while negative values represent surface erosion.

sediment fluxes for the eight sampling periods at the four monitoring sites are presented in Figure 10. In this experiment, the horizontal aeolian sediment flux increased with increasing DPs by a linear function (y=25.38x–56.56; R^2=0.472), which was consistent with the results of Zhang et al. (2011) and Pi et al. (2017). The results indicated that wind was the dominant factor affecting the wind erosion. At present, the observations of the horizontal aeolian sediment flux are scattered, and the long-term observation data are very limited. However, the observation of wind data is relatively systematic and perfect. There is a wide range of application prospects by using the wind speed and direction data to calculate the DP and then estimate the horizontal aeolian sediment flux, which is of great significance for the evaluation of regional aeolian activities.

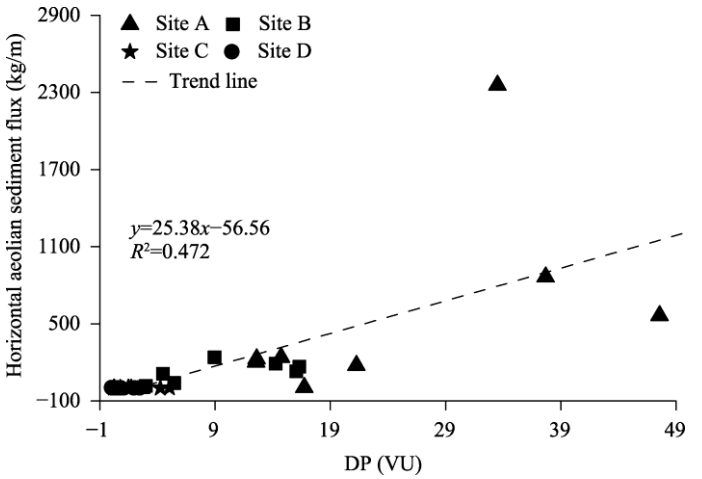

Fig. 10 Relationship between the DP and horizontal aeolian sediment flux at the four monitoring sites

4.2 Effect of vegetation on wind erosion

The soils in sparsely vegetated drylands are frequently mobilized to form sand storms (UNEP et al., 2016). Vegetation cover plays a significant role in reducing wind erosion and nutrient loss rates (Li et al., 2007). Vegetation can offer a protective cover by occupying part of the surface (King et al., 2005), binding sand with roots (Ash and Wasson, 1983), modifying wind flow (Gillies et al., 2002), and trapping aeolian sediment. Keiko and Satoshi (2007) indicated that the vibrations of flexible vegetation leaves can increase the air turbulence and thereby reduce the wind speed and sand-transport rate.

The main factors affecting the benefits of vegetation on wind prevention and sand fixation are plant morphology, vegetation height, canopy width, plant coverage, lateral cover, and plant distribution relative to the wind direction. However, vegetation coverage is the most used indicator to characterize vegetation parameters that affect the benefits of wind prevention and sand fixation. The threshold friction velocities increased as increasing vegetation coverage (Stockton and Gillette, 1990), while the surface activity intensified as decreasing vegetation coverage (Wiggs et al., 1995). The observations of dunes in Australian desert dunefield indicated that sand mobility occurred in the areas with 30% vegetation coverage (Ash and Wasson, 1983). Wiggs et al. (1995) reported that the possible threshold vegetation coverage for wind erosion control was 14% in southwestern Kalahari, Africa. The field results on the Hasaki Coast in Japan indicated that the aeolian sediment transport rate can be reduced by 95% with a vegetation coverage of 28% (Kuriyama et al., 2005). Field measurements in Owens Lake, California, showed that the sediment flux exponentially decreased with increasing vegetation coverage, and the sediment transport was effectively eliminated when the salt grass coverage was greater than 15% (Lancaster and Baas, 1998). The relationship between vegetation coverage and sediment mass flux in the wind tunnel study (Burri et al., 2011) is similar to that found for salt grass (*Distichlis spicata*) by Lancaster and Baas (1998). The field results in the Nizzana area indicated that the

effect of vegetation coverage on sand transport in the interdune corridor can be well described by an exponential function; transported mass in areas with 17% vegetation cover is less than 1% of the transported mass in non-vegetated areas and is 8% of the transported mass in areas with 9% vegetation cover (Breckle et al., 2008). Yan et al. (2013) indicated that for the Chinese semi-arid steppe, vegetation coverage should be greater than 35% to effectively protect fine particles and nutrients. However, the study of Meng et al. (2018) conducted in the grasslands of Inner Mongolia Autonomous Region in China showed that wind erosion and vegetation coverage presented a power function, and the critical vegetation coverage to control wind erosion should be greater than 60%.

The relationship between vegetation coverage and sediment flux, and the threshold vegetation coverage to control wind erosion are both different in the above results. The main reasons for the difference are the variations in surface soil structure, and the type, morphology, and distribution of plants. In this experiment, the horizontal aeolian sediment flux decreased with increasing vegetation coverage by a negative exponential function (Fig. 11), which was consistent with field results of Lancaster and Baas (1998) and Breckle et al. (2008). The total horizontal aeolian sediment flux at site C with *Artemisia ordosica* coverage of 29% during the period from 2 June 2018 to 6 June 2019 was 10.54 kg/m, which was less than 1% of that at site A with *Artemisia ordosica* coverage of 2%. The total horizontal aeolian sediment flux decreased sharply with the increase in coverage when the *Artemisia ordosica* coverage was smaller than 29%; however, it changed little with the increase in coverage when the *Artemisia ordosica* coverage was greater than 29%. Therefore, we can conclude that wind erosion would be effectively controlled when the *Artemisia ordosica* coverage is greater than 29%.

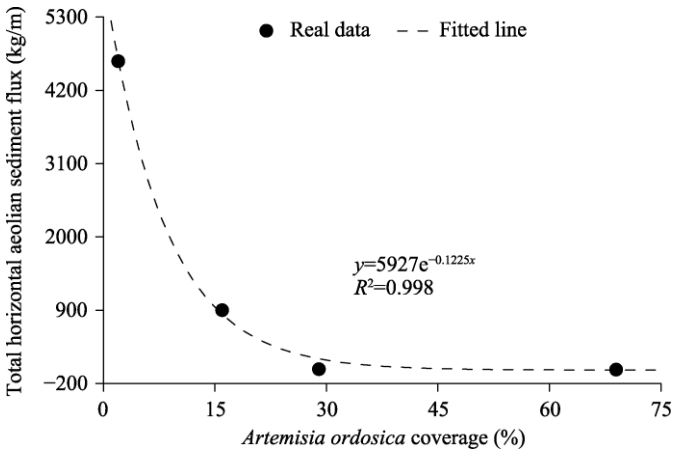

Fig. 11 Relationship between *Artemisia ordosica* coverage and the total horizontal aeolian sediment flux during the period from 2–3 June 2018 to 6 June 2019

Wind erosion is affected not only by vegetation coverage but also by plant morphology and distribution (Dupont et al., 2014). Liu et al. (2021) analyzed the effects of three different shape models (cylinders, cones, and inverted truncated cones) on the blown-sand flux by wind tunnel experiment. Dupont et al. (2014) found that shrubs trap saltating particles but trees are more efficient than shrubs in reducing sand erosion. Lateral cover, which accounts for both vegetation density and height, is a better metric of vegetation cover than coverage for evaluating wind erodibility in desert ecosystems; the lateral cover of 9% may be a key threshold for controlling wind erosion (Li et al., 2007). Vegetation canopy gap size and height are important indicators for wind erosion monitoring and management (Webb et al., 2021). Okin (2008) developed a new nonequilibrium model using the size distribution of erodible gaps between plants to characterize the ratio of the maximum shear stress to the average shear stress at the surface. Therefore, plant morphology, plant distribution, and other factors should also be considered in vegetation

construction in the Mu Us Sandy Land.

To combat desertification and air pollution and to improve regional ecological and environmental conditions, China has successively implemented many major ecological projects, such as the Three-North Shelter Forest Project, Beijing–Tianjin Sandstorm Source Control Project, Grain for Green Program, and Natural Forest Conservation Program. Artificial afforestation, aerial sowing for afforestation, enclosure, restoration and manual renewal of degraded forests, etc., have been widely carried out (National Forestry and Grassland Administration of China, 2017). Large-scale ecological restoration projects in China have been successful in curbing land degradation and improving ecosystem services (Zhao et al., 2021). China accounts for only 7% of global vegetated area but it contributes 25% of the global net increase in leaf area (Chen et al., 2019). The Mu Us Sandy Land is located in the sandstorm source area in northern China and is the key implementation area of the above-mentioned ecological projects. Due to the implementation of these ecological restoration projects, the vegetation in the Mu Us Sandy Land has been improved significantly in recent decades (Xiu et al., 2018; Xu et al., 2018). However, water resources in the Mu Us Sandy Land are also sharply decreasing; therefore, sustainable ecological restoration strategies should balance land restoration and water resources consumption (Zhao et al., 2021). The construction of vegetation in sandy land should follow the laws of nature and choose suitable species types based on natural conditions. The wind-proof and sand-fixing effects of different plant species are different. According to the characteristics of different plant species and combined with the regional wind regimes, we can determine the optimal density and coverage of vegetation, which can not only achieve the purpose of wind-proof and sand-fixing effects but also save cost and reduce regional water resources consumption.

5 Conclusions

Based on the field data of wind regimes, aeolian sediment transport, and surface changes in *Artemisia ordosica* plots with different coverages in the Mu Us Sandy Land, this study analyzed the wind-proof and sand-fixing effects of *Artemisia ordosica*. The results indicated that *Artemisia ordosica* in the Mu Us Sandy Land had significant wind-proof and sand-fixing effects. With the increase of *Artemisia ordosica* coverage, the benefit of wind-proof and sand-fixing gradually increased. The wind erosion in the Mu Us Sandy Land would be effectively controlled when the *Artemisia ordosica* coverage is greater than 29%. The main research object of this study is *Artemisia ordosica*, and it is thus recommended to conduct research on the threshold coverage of other wind-proof and sand-fixing plants for the purpose of preventing wind erosion more effectively in the future.

Acknowledgements

This study was funded by the Fundamental Research Funds of Chinese Academy of Forestry (CAFYBB2019MA009), the National Natural Science Foundation of China (41701010), the Key Special Project on 'Science and Technology Promoting the Development of Inner Mongolia Autonomous Region' (KJXM-EEDS-2020006), and the Youth Innovation Promotion Association of Chinese Academy of Sciences (2018459). We thank Prof. ZHAO Yuxing and Ms. SHI Lin from Ordos Research Institute of Forestry and Grassland Science for their help on the experiment. We are grateful for the anonymous reviewers and editors for their useful comments and valuable suggestions.

References

Asensio C, Lozano F J, Gallardo P, et al. 2016. Soil wind erosion in ecological olive trees in the Tabernas desert (southeastern Spain): a wind tunnel experiment. Solid Earth, 7(4): 1233–1242.

Ash J E, Wasson R J. 1983. Vegetation and mobility in the Australian desert dunefield. Zeitschrift für Geomorphologie, 45: 7–25.

Breckle S W, Yair A, Veste M, et al. 2008. Arid Dune Ecosystems. Heidelberg: Springer Berlin, 217–220.

Buckley R. 1987. The effect of sparse vegetation on the transport of dune sand by wind. Nature, 325(6103): 426–428.

Buckley R. 1996. Effects of vegetation on the transport of dune sand. Annals of Arid Zone, 35(3): 215–223.

Burri K, Gromke C, Lehning M, et al. 2011. Aeolian sediment transport over vegetation canopies: A wind tunnel study with live plants. Aeolian Research, 3(2): 205–213.

Chen C, Park T, Wang X H, et al. 2019. China and India lead in greening of the world through land-use management. Nature Sustainability, 2(2): 122–129.

Ci L J, Yang X H. 2010. Desertification and Its Control in China. Beijing: Higher Education Press, 299–426.

Dupont S, Bergametti G, Simoëns S. 2014. Modeling aeolian erosion in presence of vegetation. Journal of Geophysical Research-Earth Surface, 119(2): 168–187.

Feng K, Wang T, Liu S L, et al. 2021. Path analysis model to identify and analyse the causes of aeolian desertification in Mu Us Sandy Land, China. Ecological Indicators, 124: 107386, doi: 10.1016/j.ecolind.2021.107386.

Folk R L, Ward W C. 1957. Brazos River bar: a study in the significance of grain size parameters. Journal of Sedimentary Research, 27(1): 3–26.

Fryberger S G, Dean G. 1979. Dune forms and wind regime. In: McKee E D. Washington: United States Geological Survey, 137–169.

Gillies J A, Nickling W G, King J. 2002. Drag coefficient and plant form response to wind speed in three plant species: Burning Bush (*Euonymus alatus*), Colorado Blue Spruce (*Picea pungens glauca*), and Fountain Grass (*Pennisetum setaceum*). Journal of Geophysical Research: Atmospheres, 107(D24): 4760, doi: 10.1029/2001JD001259.

IPCC. 2019. Climate Change and Land: an IPCC special report on climate change, desertifcation, land degradation, sustainable land management, food security, and greenhouse gas fluxes in terrestrial ecosystems. [2021-12-20]. https://www.ipcc.ch/srccl/.

Keiko U, Satoshi T. 2007. Experimental study of blown sand in a vegetated area. Journal of Coastal Research, 23(5): 1175–1182.

King J, Nickling W G, Gillies J A. 2005. Representation of vegetation and other nonerodible elements in aeolian shear stress partitioning models for predicting transport threshold. Journal of Geophysical Research: Earth Surface, 110(F4): F04015, doi: 10.1029/2004JF000281.

Kuriyama Y, Mochizuki N, Nakashima T. 2005. Influence of vegetation on aeolian sand transport rate from a backshore to a foredune at Hasaki, Japan. Sedimentology, 52(5): 1123–1132.

Lancaster N, Baas A. 1998. Influence of vegetation cover on sand transport by wind: Field studies at Owens Lake, California. Earth Surface Processes and Landforms, 23(1): 69–82.

Leenders J K, van Boxel J H, Sterk G. 2007. The effect of single vegetation elements on wind speed and sediment transport in the Sahelian zone of Burkina Faso. Earth Surface Processes and Landforms, 32(10): 1454–1474.

Leenders J K, Sterk G, Van Boxel J H. 2011. Modelling wind-blown sediment transport around single vegetation elements. Earth Surface Processes and Landforms, 36(9): 1218–1229.

Leenders J K, Sterk G, van Boxel J H. 2016. Wind erosion reduction by scattered woody vegetation in farmers' fields in Northern Burkina Faso. Land Degradation & Development, 27(8): 1863–1872.

Lei J Q, Li S Y, Jin Z Z, et al. 2008. Comprehensive eco-environmental effects of the shelter-forest ecological engineering along the Tarim Desert Highway. Chinese Science Bulletin, 53: 190–202.

Li J R, Okin G S, Alvarez L, et al. 2007. Quantitative effects of vegetation cover on wind erosion and soil nutrient loss in a desert grassland of southern New Mexico, USA. Biogeochemistry, 85: 317–332.

Li X R, Xiao H L, Zhang J G, et al. 2004. Long-term ecosystem effects of sand-binding vegetation in the Tengger Desert, northern China. Restoration Ecology, 12(3): 376–390.

Liu J Q, Kimura R, Miyawaki M, et al. 2021. Effects of plants with different shapes and coverage on the blown-sand flux and roughness length examined by wind tunnel experiments. CATENA, 197: 104976, doi: 10.1016/j.catena.2020.104976.

Meng Z J, Dang X H, Gao Y, et al. 2018. Interactive effects of wind speed, vegetation coverage and soil moisture in controlling wind erosion in a temperate desert steppe, Inner Mongolia of China. Journal of Arid Land, 10(4): 534–547.

National Forestry and Grassland Administration of China. 2017. 2017 China Forestry and Grassland Development Report. Beijing: China Forestry Press. (in Chinese)

Ohte N, Miki N H, Matsuo N, et al. 2021. Life history of *Juniperus sabina* L. adapted to the sand shifting environment in the Mu Us Sandy Land, China: A review. Landscape and Ecological Engineering, 17(3): 281–294.

Okin G S. 2008. A new model of wind erosion in the presence of vegetation. Journal of Geophysical Research: Earth Surface, 113(F2): F02S10, doi: 10.1029/2007JF000758.

Pang Y J, Wu B, Li Y H, et al. 2020. Morphological characteristics and dynamic changes of seif dunes in the eastern margin of the Kumtagh Desert, China. Journal of Arid Land, 12(5): 887–902.

Pi H W, Sharratt B, Lei J Q. 2017. Windblown sediment transport and loss in a desert-oasis ecotone in the Tarim Basin. Scientific Reports, 7: 7723, doi: 10.1038/s41598-017-04971-4.

Stockton P H, Gillette D A. 1990. Field measurement of the sheltering effect of vegetation on erodible land surfaces. Land Degradation & Development, 2(2): 77–85.

Sun Z H, Mao Z G, Yang L Y, et al. 2021. Impacts of climate change and afforestation on vegetation dynamic in the Mu Us Desert, China. Ecological Indicators, 129: 108020, doi: 10.1016/j.ecolind.2021.108020.

Sweeney M R, Lu H Y, Cui M C, et al. 2016. Sand dunes as potential sources of dust in northern China. Science China Earth Sciences, 59: 760–769.

Udden J A. 1914. Mechanical composition of clastic sediments. Bulletin of the Geological Society of America, 25(1): 655–744.

UNEP (United Nations Environment Programme), WMO (World Meteorological Organization), UNCCD (United Nations Convention to Combat Desertification). 2016. Global Assessment of Sand and Dust Storms. Nairobi, Kenya: UNEP. [2021-12-28]. https://library.wmo.int/doc_num.php?explnum_id=3083.

Wang T. 2003. Desert and Desertification in China. Shijiazhuang: Hebei Science & Technology Press. (in Chinese)

Webb N P, McCord S E, Edwards B L, et al. 2021. Vegetation canopy gap size and height: Critical indicators for wind erosion monitoring and management. Rangeland Ecology & Management, 76(1): 78–83.

Wentworth C K. 1922. A scale of grade and class terms for clastic sediments. The Journal of Geology, 30(5): 377–392.

Wiggs G F S, Thomas D S G, Bullard J E, et al. 1995. Dune mobility and vegetation cover in the Southwest Kalahari Desert. Earth Surface Processes and Landforms, 20(6): 515–529.

Wolfe S A, Nickling W G. 1993. The protective role of sparse vegetation in wind erosion. Progress in Physical Geography, 17(1): 50–68.

Xiu L N, Yan C Z, Li X S, et al. 2018. Monitoring the response of vegetation dynamics to ecological engineering in the Mu Us Sandy Land of China from 1982 to 2014. Environmental Monitoring and Assessment, 190: 543, doi: 10.1007/s10661-018-6931-9.

Xu Z W, Hu R, Wang K X, et al. 2018. Recent greening (1981–2013) in the Mu Us dune field, north-central China, and its potential causes. Land Degradation & Development, 29(5): 1509–1520.

Yan Y C, Xin X P, Xu X L, et al. 2013. Quantitative effects of wind erosion on the soil texture and soil nutrients under different vegetation coverage in a semiarid steppe of northern China. Plant and Soil, 369: 585–598.

Youssef F, Visser S M, Karssenberg D, et al. 2012. The effect of vegetation patterns on wind-blown mass transport at the regional scale: A wind tunnel experiment. Geomorphology, 159: 178–188.

Zhang M M, Wu X Q. 2020. The rebound effects of recent vegetation restoration projects in Mu Us Sandy land of China. Ecological Indicators, 113: 106228, doi: 10.1016/j.ecolind.2020.106228.

Zhang Z C, Dong Z N, Zhao A G, et al. 2011. Relationship between sand transport and sand drift potential. Journal of Desert Research, 31(4): 824–827. (in Chinese)

Zhao M, Geruo G, Zhang J, et al. 2021. Ecological restoration impact on total terrestrial water storage. Nature Sustainability, 4: 56–62.